ELSEVIER

Journal of Organometallic Chemistry 529 (1997) 343–350

Journal of Organometallic Chemistry

Bis- and tetrakis-(diphenylphosphino)tetrathiafulvalenes as precursors of redox-active organic–inorganic polymeric networks

M. Fourmigué [a,*], C.E. Uzelmeier [b], K. Boubekeur [a], S.L. Bartley [b], K.R. Dunbar [b]

[a] *Institut des Matériaux (IMN, UMR CNRS 110), 2, rue de la Houssinière, F-44072 Nantes Cedex 03, France*
[b] *Department of Chemistry, Michigan State University, East Lansing, MI 48824, USA*

Received 22 March 1996

Abstract

Lithiation of the (*Z*)-, (*E*)-dimethyltetrathiafulvalene mixture and subsequent reaction with $ClPPh_2$ afford (*Z*)- and (*E*)-dimethylbis(diphenylphosphino)tetrathiafulvalene which are separated by fractional recrystallization. The identity of (*Z*)-$\mathbf{P_2}$ has been ascertained by its X-ray crystal structure determination. By similar methods, tetrakis(diphenylphosphino)tetrathiafulvalene ($\mathbf{P_4}$) is obtained from the tetrathiafulvalene tetralithium derivative. Cyclic voltammetry experiments reveal that the new compounds oxidize reversibly in two one-electron steps to the radical cation and dication. Reaction of *o*-$\mathbf{P_2}$ with the dinuclear complex $[Rh_2(NCCH_3)_{10}](BF_4)_4$ has been investigated and found to produce the square-planar Rh(I) compound $[(o\text{-}\mathbf{P_2})_2Rh][BF_4]$. The identity of the product has been confirmed by X-ray crystallography, FAB-MS, elemental analysis, and NMR spectroscopy. Several reactions of solvated cations were also performed, all of which appear to lead to products with *o*-$\mathbf{P_2}$ and $\mathbf{P_4}$ ligands.

Keywords: Tetrathiafulvalene; Rhodium; Phosphines; Crystal structure; Polymers

1. Introduction

Incorporation of transition metal ions into a conjugated polymer backbone to form coordination polymers is the subject of considerable interest in view of the possible electrical and magnetic properties of such chains. Thus, it has been reasoned that the introduction of metal ions in a conjugated chain could lead to partially-filled bands and possibly metallic conductivity [1]. Ferrimagnetic polymer chains with magnetic metal ions (Cu^{2+}, Mn^{3+}) have been shown to order ferromagnetically [2]. Recently, emphasis has been placed on the use of open-shell ligands such as semiquinones [3], nitronyl nitroxides [4] or nitroxides [5] which provide a coordinating functionality (bi-, tri-, or tetradentate) with a simultaneous contribution to the electronic and/or magnetic properties of the whole composite chain.

In this vein, suitably designed multidentate ligands bearing the extra redox functionality of a tetrathiafulvalene (TTF) core are particularly attractive. They include both the capability of the TTF core to be readily oxidized to the cation radical and the coordinating ability of the selected TTF substituents. We recently demonstrated that phosphorus(III) compounds could be readily prepared from tetrathiafulvalenyl lithium derivatives and reported, for example, the preparation of the chelating 3,4-dimethyl-3′,4′-bis(diphenylphosphino)tetrathiafulvalene (*o*-$\mathbf{P_2}$) [6] (Scheme 1).

The chelating ability of this diphosphine was demonstrated by the isolation of NiX_2 complexes of general formula $[o\text{-}\mathbf{P_2}]NiX_2$ (structure (aa) in Scheme 2). In order to be able to build polymeric structures based on metal–phosphine complexes (such as (c) or (cc) in Scheme 2), two ingredients are required: (i) a bridging diphosphine or tetraphosphine, (ii) a metal center capable of coordinating two phosphines (b, c) or two diphosphines (bb, cc).

In this paper we report that *o*-$\mathbf{P_2}$ can be used as the sole ligand in mononuclear metal complexes bearing two such diphosphines (structure (bb) in Scheme 1), a prerequisite for the elaboration of extended polymeric complexes of structure (cc). Indeed, the preparation of the required tetraphosphine tetrakis(diphenylphosphino)tetrathiafulvalene ($\mathbf{P_4}$) allows for the isolation of the corresponding extended structure of type (cc), $[(\mathbf{P_4})M]_n$. Additionally, the bridging diphosphine that is

* Corresponding author.

0022-328X/97/$17.00 © 1997 Elsevier Science S.A. All rights reserved.
PII S0022-328X(96)06637-5

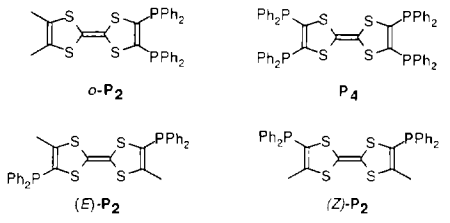

Scheme 1.

required for the elaboration of type (c) polymer, the (*E*)-dimethyl-bis(diphenylphosphino)tetrathiafulvalene, (*E*)-$\mathbf{P_2}$, is described, together with the (*Z*) isomer. While polymers can be expected from the coordination chemistry of the (*E*)-$\mathbf{P_2}$ isomer, the (*Z*)-$\mathbf{P_2}$ isomer could lead to cyclic oligomers or helical structures.

2. Results and discussion

A preliminary report of this work has appeared in Ref. [7].

2.1. Synthesis, $^{31}P\{^1H\}$ NMR spectroscopy and redox properties of the TTF-containing phosphines

The most general procedures for substituting the TTF core take advantage of the acidity of the TTF hydrogen atoms [8]. Thus, treatment with strong bases such as lithiumdiisopropylamide (LDA) at −78 °C affords TTF–Li which can be reacted with a variety of electrophiles. Using this procedure, we earlier reported the preparation of several TTF derivatives substituted with one PPh_2 group from the reaction of the corresponding lithium derivative, TTF–Li [6], *o*-Me_2TTF–Li [9] or Me_3TTF–Li [10] with $ClPPh_2$. Also, reaction with di- or trihalides, such as $PhPCl_2$ or PBr_3, afforded phosphines bearing two [11] or three [12] such tetrathiafulvalenyl redox moieties. In order to prepare diphosphines with the two $-PPh_2$ groups on the same or on opposite dithiole rings, access to the corresponding dilithio TTF compound was required. However, as shown by Green [8], treatment of TTF itself with two equivalents of

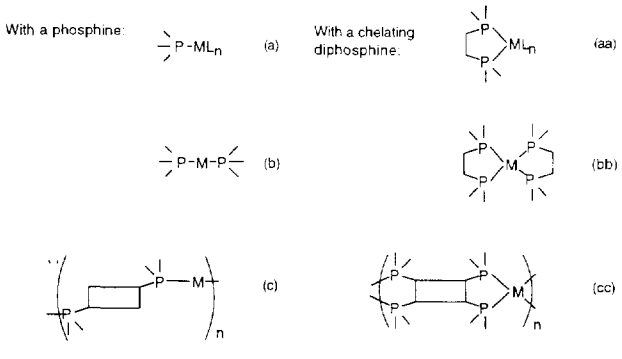

Scheme 2.

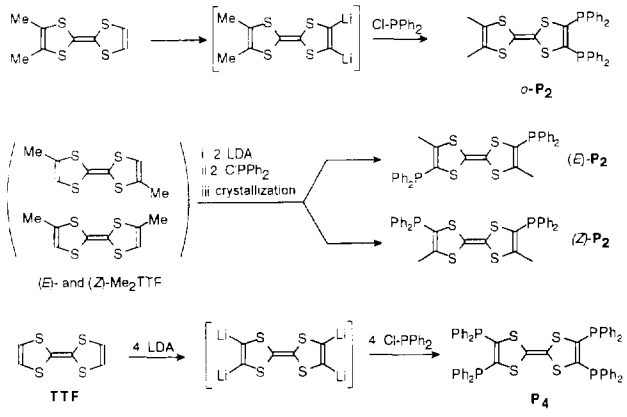

Scheme 3.

LDA leads to a complex mixture of polylithiated species. This difficulty was successfully circumvented for the preparation of *o*-$\mathbf{P_2}$ by using the unsymmetrically substituted *o*-Me_2TTF [6] (Scheme 3).

A similar strategy was employed here for the preparation of (*E*)- and (*Z*)-$\mathbf{P_2}$, starting from the dimethyl-substituted TTF, available as an inseparable mixture of the (*Z*) and (*E*) isomers. Reaction of this (*Z*),(*E*)-Me_2TTF mixture with two equivalents of LDA, followed by addition of two equivalents of $ClPPh_2$ afforded the mixture of (*Z*)- and (*E*)-$\mathbf{P_2}$ in 55% overall yield. The two isomers could not be distinguished on the basis of TLC, but recrystallization of the crude product from toluene afforded one crystalline product (m.p. 236–239 °C) while concentration of the mother liquor and slow addition of methanol yielded long needles of a second product (m.p. 192–194 °C). Mass spectroscopy and elemental analysis confirm the $C_{32}H_{26}P_2S_4$ formula expected for both isomers, while the ^1H and $^{31}P\{^1H\}$ NMR spectra proved to be identical. The single crystal X-ray structural determination of the second product (see below) demonstrated that it was in fact the (*Z*) isomer, as one could indeed expect for this less symmetrical compound whose melting point is lower and solubility higher than those of the (*E*) isomer. Furthermore, tetralithiation of TTF has been shown to be readily achieved with an excess of LDA in THF [13]; subsequent derivatization with $ClPPh_2$ affords $\mathbf{P_4}$ in good yield.

$^{31}P\{^1H\}$ NMR spectroscopic data (Table 1) show that the ^{31}P chemical shift of the phosphines is affected by the electron-rich character of the TTF moiety if one compares those values with that of PPh_3 for example (−6 ppm).

Table 1
$^{31}P\{^1H\}$ NMR data for the various phosphines

	o-$\mathbf{P_2}$	$\mathbf{P_4}$	$\mathbf{P_1}$	(*Z*)-$\mathbf{P_2}$	(*E*)-$\mathbf{P_2}$
δ (ppm)	−18.8	−18.2	−22.7	−18.3	−18.3

Table 2
Cyclic voltammetry data of the free ligands (in CH_2Cl_2, n-Bu_4NPF_6 0.1 M, 100 mV s^{-1}, Fc^+/Fc at 0.39 V)

Donor	$E1_{1/2}$ (V vs. SCE)	$E2_{1/2}$ (V vs. SCE)
TMTTF	0.21	0.56
$\mathbf{P_1}$	0.23	0.74
o-$\mathbf{P_2}$	0.27	0.81
(Z)-$\mathbf{P_2}$	0.31	0.76
(E)-$\mathbf{P_2}$	0.31	0.76
$\mathbf{P_4}$	0.33	0.73

As shown by cyclic voltammetry experiments, all new compounds exhibit two reversible one-electron oxidations to the mono- and dication. Compared with the reported data for tetramethyltetrathiafulvalene (TMTTF), it appears that the substitution of $-PPh_2$ groups for methyl groups only slightly decreases their donor properties (Table 2). These molecules should then retain the redox ability of the TTF core, the added coordination ability not withstanding.

2.2. X-ray crystal structure of (Z)-$\mathbf{P_2}$

The crystallographic data for (Z)-$\mathbf{P_2}$ are given in Table 3. Table 4 contains the atomic coordinates and equivalent isotropic displacement coefficients. Selected bond distances and angles are given in Table 5. Fig. 1 shows the structure of (Z)-$\mathbf{P_2}$ confirming the (Z) stereochemistry. (Z)-$\mathbf{P_2}$ was found to crystallize together with one toluene solvent molecule disordered on the symmetry center. Bond distances and angles within the TTF moiety are in accord with those of other TTF molecules. The TTF core itself is nearly planar with dihedral angles between planes (C1,C2,S1,S2) and (S1,S2,C4,C5,S3,S4) of 3.7(2)° and between planes (S1,S2,C4,C5,S3,S4) and (S3,S4,C6,C7) of 0.9(1)°. The two phosphorus atoms adopt the usual distorted tetrahedral environment with C–P–C angle values of 101.7–103.7°

3. Metal complexes with o-$\mathbf{P_2}$ and $\mathbf{P_4}$

3.1. Synthesis, spectroscopy and redox properties of [Rh(o-$\mathbf{P_2}$)$_2$][BF_4] (1)

Several years ago, we have already reported the preparation and electrochemical behavior of coordination complexes of o-$\mathbf{P_2}$ with nickel halides such as o-$\mathbf{P_2}\cdot NiCl_2$ and o-$\mathbf{P_2}\cdot NiBr_2$ [6]. In this paper we wish to report the results of our investigations with acetonitrile-coordinated cations of the platinum group metals, including the metal–metal bonded cation $[Rh_2(NCCH_3)_{10}]^{4+}$ [14] with the chelating diphosphines o-$\mathbf{P_2}$ or $\mathbf{P_4}$.

The reaction of four equivalents of o-$\mathbf{P_2}$ with $[Rh_2(NCCH_3)_{10}][BF_4]_4$ in CH_3CN affords the mononuclear complex [Rh(o-$\mathbf{P_2}$)$_2$][BF_4] (**1**) as yellow microcrystals in 76% yield. The yellow solid is insoluble in most common solvents and exhibits only limited solubility in CH_2Cl_2 and acetone. The infrared spectrum of (**1**) displays bands attributed to the phosphine ligand along with stretches assignable to $[BF_4]^-$ ions. The absence of ν(C≡N) stretches supports the loss of all CH_3CN ligands. The FAB mass spectrum exhibits a

Table 3
Crystallographic data for (Z)-$\mathbf{P_2}$ and [o-$\mathbf{P_2}$]$_2$RhBF$_4$

	(Z)-$\mathbf{P_2}\cdot PhCH_3$	[o-$\mathbf{P_2}$]$_2$RhBF$_4\cdot 5H_2O$
Empirical formula	$C_{32}H_{26}P_2S_4$	$C_{64}H_{52}BF_4P_4RhS_8\cdot O_5H_{10}$
Formula weight (g mol^{-1})	600.742	1481.33
Crystal color and shape	orange plate	yellow plate
Crystal size (mm^3)	0.33 × 0.30 × 0.09	0.3 × 0.2 × 0.1
Cystal system	triclinic	monoclinic
Space group	$P\bar{1}$	$C2/c$
Unit cell dimensions		
a (Å)	9.362(5)	15.761(2)
b (Å)	14.204(3)	19.007(2)
c (Å)	14.265(1)	24.736(2)
α (deg)	108.02(1)	
β (deg)	102.22(2)	107.31(1)
γ (deg)	106.35(2)	
Volume (Å^3)	1635(1)	7100(1)
Z	2	4
Density (calc.) (g cm^{-3})	1.313	1.408
Absorption coeff. (mm^{-1})	0.41	0.62
R	0.048	0.16
Rw	0.065	0.21
Weighting scheme	$(\sigma^2(F_o)+(0.0025F_o^2)^{-1}$	$(\sigma^2(F_o)+(0.0064F_o^2)^{-1}$
Max res. electron density (e Å^{-3})	0.54	4.3

Table 4
Atomic coordinates and equivalent isotropic displacement coefficients for (*Z*)-$\mathbf{P_2}\cdot PhCH_3$

	x	*y*	*z*	U_{eq}
S1	0.5923(1)	0.3538(1)	0.2746(1)	0.0501(6)
S2	0.7807(1)	0.5136(1)	0.4872(1)	0.0553(6)
S3	0.5532(2)	0.3816(1)	0.5825(1)	0.0573(6)
S4	0.3578(2)	0.2237(1)	0.3715(1)	0.0542(6)
P1	0.7876(2)	0.4830(1)	0.1724(1)	0.0477(6)
P2	0.1328(1)	0.0876(1)	0.4555(1)	0.0455(6)
C1	0.7479(5)	0.4650(4)	0.2866(4)	0.044(2)
C2	0.8328(6)	0.5377(4)	0.3840(4)	0.048(2)
C3	0.9706(7)	0.6371(4)	0.4136(4)	0.065(3)
C4	0.6176(5)	0.3952(4)	0.4085(4)	0.045(2)
C5	0.5223(5)	0.3414(4)	0.4486(4)	0.048(2)
C6	0.3003(5)	0.2035(4)	0.4761(4)	0.042(2)
C7	0.3918(5)	0.2761(4)	0.5719(4)	0.044(2)
C8	0.3726(6)	0.2790(4)	0.6747(4)	0.060(3)
C9	0.6364(6)	0.3633(4)	0.0653(4)	0.048(2)
C10	0.6492(7)	0.2666(5)	0.0245(5)	0.087(3)
C11	0.5274(9)	0.1821(5)	−0.0583(6)	0.099(4)
C12	0.3930(8)	0.1936(6)	−0.0996(5)	0.087(4)
C13	0.3782(7)	0.2882(7)	−0.0625(5)	0.084(4)
C14	0.4977(7)	0.3734(5)	0.0198(5)	0.064(3)
C15	0.9640(5)	0.4520(4)	0.1761(4)	0.047(2)
C16	1.0070(6)	0.3877(4)	0.2237(4)	0.056(3)
C17	1.1404(7)	0.3663(5)	0.2188(5)	0.067(3)
C18	1.2315(7)	0.4081(5)	1.7676(5)	0.076(3)
C19	1.1942(7)	0.4735(6)	0.1223(5)	0.076(3)
C20	1.0591(6)	0.4949(4)	0.1264(4)	0.061(3)
C21	0.1738(6)	−0.0216(4)	0.3724(4)	0.048(2)
C22	0.0531(6)	−0.1151(4)	0.3009(4)	0.060(3)
C23	0.0846(7)	−0.2025(4)	0.2474(5)	0.074(3)
C24	0.2344(8)	−0.1980(5)	0.2642(6)	0.087(4)
C25	0.3567(7)	−0.1059(5)	0.3335(6)	0.087(4)
C26	0.3280(6)	0.0180(4)	0.3900(5)	0.066(3)
C27	−0.0310(5)	0.0946(3)	0.3652(4)	0.044(2)
C28	−0.0386(6)	0.0920(4)	0.2656(4)	0.055(2)
C29	−0.1614(7)	0.1031(4)	0.2057(4)	0.066(3)
C30	−0.2831(7)	0.1161(4)	0.2415(5)	0.072(3)
C31	−0.2808(6)	0.1164(5)	0.3378(6)	0.071(3)
C32	−0.1552(6)	0.1055(4)	0.3997(4)	0.056(3)
C33	0.064(2)	0.0904(9)	0.010(1)	0.125(9)
C34	0.216(2)	0.003(2)	0.0919(8)	0.20(1)
C35 *	0.073(2)	0.011(2)	0.029(1)	0.12(1)
C36 *	−0.065(6)	0.098(3)	−0.046(3)	0.18(3)
C37 *	0.200(3)	0.089(2)	0.071(2)	0.13(1)

Starred (*) atoms have a site occupation factor of 0.5.

Table 5
Important bond distances and angles in (*Z*)-$\mathbf{P_2}$

S1–C1	1.755(5)	P1–C15	1.820(6)
S1–C4	1.757(5)	P2–C6	1.819(5)
S2–C2	1.744(6)	P2–C21	1.831(6)
S2–C4	1.755(4)	P2–C27	1.830(5)
S3–C5	1.748(5)	C1–C2	1.346(6)
S3–C7	1.744(5)	C2–C3	1.487(7)
S4–C5	1.752(4)	C4–C5	1.346(8)
S4–C6	1.766(6)	C6–C7	1.342(5)
P1–C1	1.821(6)	C7–C8	1.504(8)
P1–C9	1.831(4)		
C1–S1–C4	95.7(2)	S2–C2–C3	115.8(4)
C2–S2–C4	95.6(2)	C1–C2–C3	126.3(6)
C5–S3–C7	96.0(2)	S1–C4–S2	114.1(3)
C5–S4–C6	96.0(2)	S1–C4–C5	123.6(3)
C1–P1–C9	102.2(2)	S2–C4–C5	122.3(4)
C1–P1–C15	101.9(3)	S3–C5–S4	114.0(3)
C9–P1–C15	101.8(2)	S3–C5–C4	122.9(3)
C6–P2–C21	101.7(2)	S4–C5–C4	123.0(4)
C6–P2–C27	103.6(2)	S4–C6–P2	121.9(2)
C21–P2–C27	103.1(2)	S4–C6–C7	116.0(4)
S1–C1–P1	121.5(2)	P2–C6–C7	122.0(4)
S1–C1–C2	116.6(5)	S3–C7–C6	118.0(4)
P1–C1–C2	121.9(4)	S3–C7–C8	114.2(3)
S2–C2–C1	117.9(4)	C6–C7–C8	127.7(5)

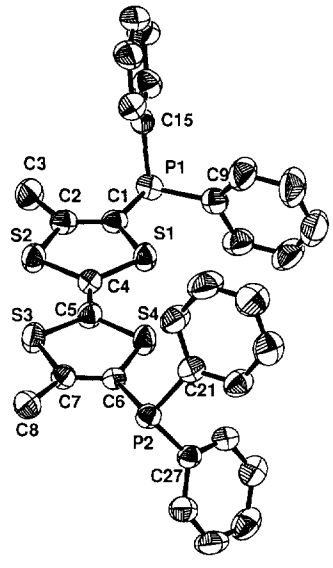

Fig. 1. ORTEP view of (*Z*)-$\mathbf{P_2}$. Thermal ellipsoids are draw at the 50% probability level.

mass at $m/z = 1303$ (M^+) that corresponds to the Rh(o-$\mathbf{P_2}$)$^+$ molecular fragment. A $^{19}F\{^1H\}$ NMR spectrum exhibits a singlet at $\delta = -154.9$ ppm which is in the range expected for the $[BF_4]^-$ ion [15]. The ^1H NMR spectrum of (**1**) contains resonances assignable only to protons of the o-$\mathbf{P_2}$ ligands, which includes a set of resonances between $\delta = 7.0$ and 7.5 ppm assigned to the phenyl protons, and a singlet at $\delta = 1.82$ ppm due to the methyl protons. The $^{31}P\{^1H\}$ NMR spectrum displays a doublet at $\delta = 50.4$ ppm with $^1J_{Rh-P} = 133.8$ Hz. These values are within the range observed for other Rh–P complexes and also compare well with the value reported for the complex o-$\mathbf{P_2}\cdot NiCl_2$ [6]. A cyclic

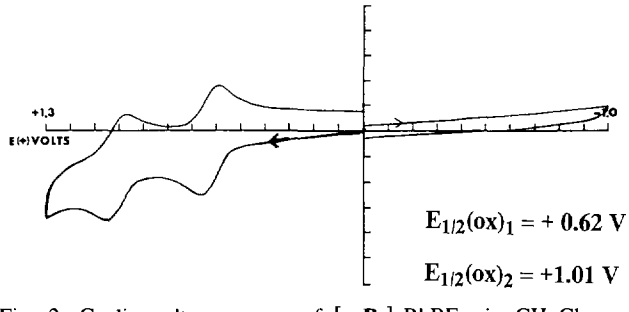

Fig. 2. Cyclic voltamogramm of $[o\text{-}\mathbf{P_2}]_2RhBF_4$, in CH_2Cl_2, vs. Ag/AgCl.

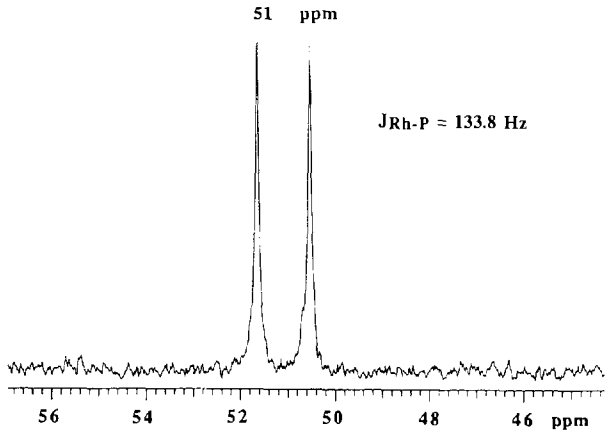

Fig. 3. $^{31}P\{^1H\}$ NMR spectrum of $[Rh^I(\mathbf{P_4})_n][BF_4]_n$ in CD_3CN at room temperature.

voltammogram of (**1**) (Fig. 2) exhibits two reversible oxidations at $E_{1/2(ox)} = 0.63$ and $E_{1/2(ox)} = 1.01$ V vs. Ag/AgCl, compared with the cyclic voltammogram of *o*-$\mathbf{P_2}$ under the same conditions which exhibits oxidations at $E_{1/2(ox)} = 0.41$ and $E_{1/2(ox)} = 0.85$ V vs. Ag/AgCl. The shift to more positive potentials of the values in (**1**) is the result of strong Rh–P interactions.

The reaction of *o*-$\mathbf{P_2}$ and the solvated Rh dinuclear complex produces the mononuclear product (**1**) as a result of reduction of the Rh^{II} (d^7) to Rh^I (d^8). As expected the d^8 Rh^I compound is diamagnetic. The reduction of the metal is accompanied by oxidation of one equivalent of ligand, justifying the need for the addition of two equivalents excess *o*-$\mathbf{P_2}$. The presence of the oxidized ligand was detected by the color change to green which is the typical color of the TTF cation.

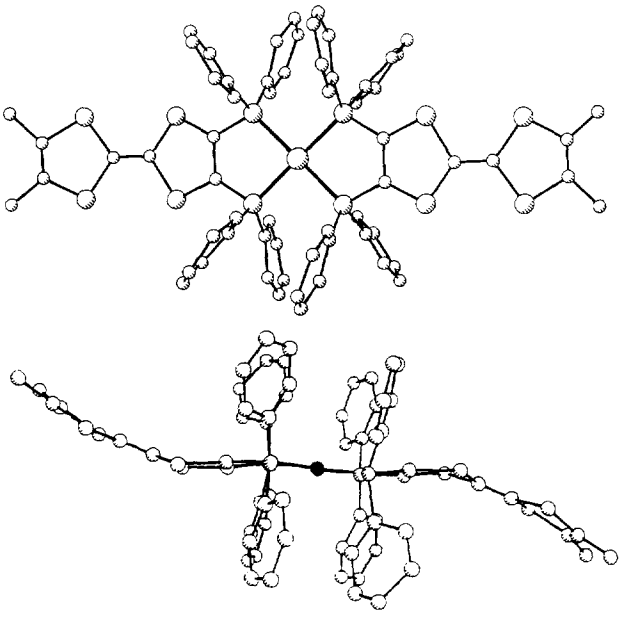

Fig. 4. PLUTO views of $[o\text{-}\mathbf{P_2}]_2Rh^+$ in $[o\text{-}\mathbf{P_2}]_2RhBF_4$.

Preliminary studies of the analogous tetradendate $\mathbf{P_4}$ ligand with $[Rh_2(NCCH_3)_{10}][BF_4]_4$ indicate that a similar reduction of the metal center occurs with subsequent binding of the ligand through the phosphine atoms. The $^{31}P\{^1H\}$ NMR spectrum displays a doublet at $\delta = 51.0$ ppm with $^1J_{Rh-P} = 133.8$ Hz, indicating only one environment for the phosphorus (Fig. 3). The ^1H NMR spectrum contains resonances assignable only to the phenyl protons, which are assigned to two broad reso-

Table 6
Atomic coordinates and equivalent isotropic displacement coefficients for $[o\text{-}\mathbf{P_2}]_2RhBF_4 \cdot 5H_2O$

	x	*y*	*z*	U_{eq}
Rh	0.00000	0.00000	0.50000	0.018(1)
S1	0.3050(5)	0.0837(4)	0.5021(4)	0.037(4
S2	0.3191(5)	−0.0659(4)	0.5295(4)	0.036(4)
S3	0.5159(5)	0.1026(4)	0.5594(4)	0.044(5)
S4	0.5355(5)	−0.0442(4)	0.5894(4)	0.041(4)
P1	0.1017(4)	0.0855(4)	0.4981(3)	0.017(3)
P2	0.1188(5)	−0.0745(4)	0.5258(3)	0.019(3)
C1	0.129(2)	0.151(1)	0.556(1)	0.029(7)
C2	0.096(2)	0.136(1)	0.601(1)	0.026(6)
C3	0.121(2)	0.179(1)	0.650(1)	0.030(7)
C4	0.165(2)	0.240(2)	0.649(2)	0.053(9)
C5	0.204(2)	0.252(2)	0.602(1)	0.046(9)
C6	0.185(2)	0.207(2)	0.556(1)	0.040(8)
C7	0.093(2)	0.130(1)	0.431(1)	0.018(6)
C8	0.096(2)	0.093(2)	0.385(1)	0.043(8)
C9	0.090(3)	0.123(2)	0.336(2)	0.06(1)
C10	0.068(3)	0.195(2)	0.329(2)	0.06(1)
C11	0.058(2)	0.231(2)	0.376(1)	0.044(8)
C12	0.069(2)	0.205(1)	0.424(1)	0.027(7)
C13	0.115(2)	−0.149(1)	0.480(1)	0.020(6)
C14	0.129(2)	−0.141(2)	0.423(1)	0.050(9)
C15	0.110(2)	−0.194(1)	0.388(1)	0.025(6)
C16	0.082(2)	−0.262(1)	0.401(1)	0.030(7)
C17	0.079(2)	−0.274(2)	0.458(1)	0.035(7)
C18	0.091(2)	−0.217(2)	0.497(1)	0.030(7)
C19	0.155(2)	−0.107(1)	0.598(1)	0.027(7)
C20	0.115(2)	−0.069(2)	0.636(1)	0.039(8)
C21	0.141(3)	−0.092(2)	0.692(2)	0.07(1)
C22	0.199(3)	−0.145(2)	0.710(2)	0.08(1)
C23	0.236(3)	−0.181(2)	0.670(2)	0.07(1)
C24	0.213(2)	−0.159(1)	0.617(1)	0.029(7)
C25	0.205(2)	0.043(1)	0.506(1)	0.02(1)
C26	0.217(2)	−0.029(1)	0.522(1)	0.02(1)
C27	0.376(2)	0.013(1)	0.533(1)	0.03(1)
C28	0.458(2)	0.025(1)	0.555(1)	0.03(1)
C29	0.616(2)	0.079(2)	0.610(1)	0.05(2)
C30	0.625(2)	0.013(2)	0.622(2)	0.05(2)
C31	0.678(3)	0.136(2)	0.634(2)	0.07(2)
C32	0.701(3)	−0.029(2)	0.665(2)	0.07(2)
B1	1.00000	0.063(2)	0.75000	0.15270
F1	1.00000	0.134(2)	0.75000	0.15270
F2 *	1.032(6)	0.042(3)	0.707(3)	0.15270
F3 *	0.915(3)	0.040(3)	0.735(4)	0.15270
F4 *	1.043(5)	0.035(3)	0.798(2)	0.15270
O1	0.50000	0.208(1)	0.25000	0.034(7)
O2	0.879(2)	0.641(1)	0.7475(9)	0.054(6)
O3	0.813(2)	0.532(1)	0.663(1)	0.070(8)

Starred (*) atoms have a site occupation factor of 0.5.

Table 7
Important bond distances and angles in $[o\text{-}\mathbf{P}_2]_2RhBF_4$

Rh–P1	2.297(7)	P1–C7	1.83(3)
Rh–P2	2.286(7)	P1–C25	1.77(3)
S1–C25	1.78(3)	P2–C13	1.80(3)
S1–C27	1.78(3)	P2–C19	1.83(3)
S2–C26	1.71(3)	P2–C26	1.80(3)
S2–C27	1.73(3)	C25–C26	1.44(4)
S3–C28	1.72(3)	C27–C28	1.27(4)
S3–C29	1.76(3)	C29–C30	1.28(5)
S4–C28	1.82(3)	C29–C31	1.46(5)
S4–C30	1.78(3)	C30–C32	1.56(5)
P1–C1	1.85(3)		
P1–Rh–P2	85.9(2)	P1–C1–C6	121(2)
P1–Rh–P2′ [a]	94.1(2)	S1–C25–P1	127(2)
C25–S1–C27	96(1)	S1–C25–C26	112(2)
C26–S2–C27	96(1)	P1–C25–C26	120(2)
C28–S3–C29	99(2)	S2–C26–P2	126(2)
C28–S4–C30	95(1)	S2–C26–C25	118(2)
Rh–P1–C1	117(1)	P2–C26–C25	115(2)
Rh–P1–C7	118.8(8)	S1–C27–S2	113(1)
Rh–P1–C25	107.5(9)	S1–C27–C28	118(2)
C1–P1–C7	109(1)	S2–C27–C28	129(2)
C1–P1–C25	103(1)	S3–C28–S4	109(1)
C7–P1–C25	97(1)	S3–C28–C27	129(2)
Rh–P2–C13	116.1(8)	S4–C28–C27	121(2)
Rh–P2–C19	119(1)	S3–C29–C30	115(2)
Rh–P2–C26	109.5(9)	S3–C29–C31	116(3)
C13–P2–C19	107(1)	C30–C29–C31	129(3)
C13–P2–C26	103(1)	S4–C30–C29	119(2)
C19–P2–C26	101(1)	S4–C30–C32	110(2)
P1–C1–C2	115(2)	C29–C30–C32	132(3)

[a] Symmetry operation used to generate equivalent atoms: $-x, -y, 1-z$.

nances at $\delta = 7.0$ and 7.3 ppm. Similar results have been observed in reactions between the $\mathbf{P}_4$ ligand and several mononuclear solvated cations of general formula $[M(NCCH_3)_n][BF_4]_2$ (M = Ni, $n = 6.5$; M = Fe, Co [16], Pd [17], $n = 6$, Pt [18], $n = 4$). Assigning these resonances to bound phosphine is justified by their considerable downfield shift with respect to $\delta = -18$ ppm for the free ligand. All the metal centers, except Co, exhibit $^{31}P\{^1H\}$ NMR spectra with a single resonance in the region of $\delta = 36$–55 ppm. SQUID measurements of the paramagnetic cobalt-complex display a $\mu_{eff} = 4.6$ BM at room temperature. Although no formal structural assignments can be made from these NMR spectra, it does support the possibility that these ligands are forming extended structures.

3.2. X-ray crystal structure of $[Rh(o\text{-}\mathbf{P}_2)_2][BF_4]$

The X-ray crystal structure of $[Rh(o\text{-}\mathbf{P}_2)_2][BF_4]$ (**1**) depicted in Fig. 4 reveals a square planar arrangement of ligands around the Rh^I center. Table 6 contains the atomic coordinates and equivalent isotropic displacement coefficients. Selected bond distances and angles are given in Table 7. The average Rh–P distance is 2.292(8) Å and the P(1)–Rh–P(2) angle is 85.9(2)°, while the P(1)–Rh–P(1)′ angle is 94.1(2)° as required by symmetry. The TTF moiety is strongly folded along the S ··· S axis of one dithiole ring by 24.2(2)°. Such deformations are not unusual and have already been observed in several non-oxidized TTF derivatives [12,19] or tetrathiafulvalenophanes [20,21]. The packing diagram of (**1**) shown in Fig. 5 reveals close intermolecular interactions between the outer dithiole rings of the TTF moieties of neighboring molecules with a plane-to-plane distance of 3.537(2) Å, resulting in the observation of one-dimensional chains parallel to the [100] direction. Those chains are isolated from each other, in the [010] as in the [001] direction, by the phenyl rings of the diphenylphosphino groups of $\mathbf{P}_2$. It is apparent from examining the packing diagram that the considerable

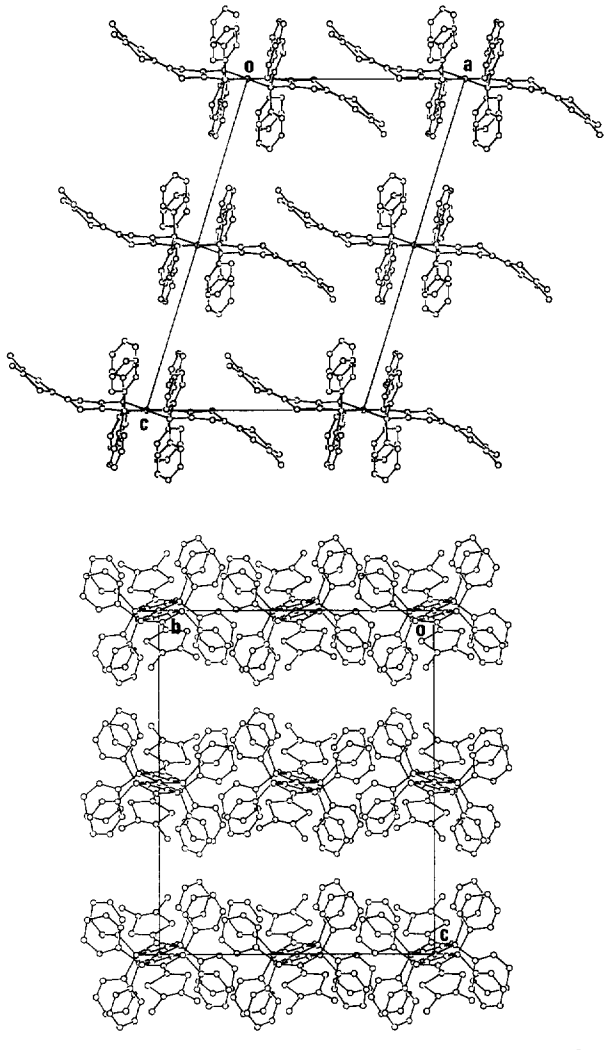

Fig. 5. Top: projection of the unit cell of $[o\text{-}\mathbf{P}_2]_2RhBF_4$ along [010]. Bottom: projection along [100]. Molecules in the central column are at $a = 1/2$. The disordered BF_4^- anions and the solvent molecules have been ommited for clarity.

bending of the TTF ligands away from the Rh–P plane is necessary for accommodating this interaction, the bulky phenyl rings preventing a perfect planar TTF–TTF intermolecular interaction. The structure of (*o*-**P$_2$**)·$NiBr_2$, unlike that of (**1**), exhibits a planar structural arrangement with respect to the Ni–**P$_2$**–TTF plane [6]. There was no evidence for intermolecular interactions occurring in the Ni complex.

The structural arrangement observed in [Rh(*o*-**P$_2$**)$_2$][BF_4] demonstrates that, despite the presence of the bulky phenyl rings, extended arrays with TTF · · · TTF overlaps can be constructed, while the electrochemical data confirm that the reversible redox character of the TTF moieties is retained in the phosphines and in their metal complexes. The introduction of paramagnetic species, either by TTF oxidation or by substituting a paramagnetic metal cation for the Rh^I metal center, offer now rich opportunities for the elaboration of novel conductive or magnetic materials.

4. Experimental

4.1. Synthesis

TTF [22] and *cis–trans*-Me_2TTF [23] were prepared according to published procedures and purified by recrystallization followed by vacuum sublimation.

4.1.1. 3,3'-Dimethyl-4,4'-bis(diphenylphosphino)tetrathiafulvalene and 3,4'-dimethyl-3',4-bis(diphenylphosphino)tetrathiafulvalene, cis- and trans-P$_2$

To a solution of the *cis–trans* mixture of Me_2TTF (1.05 g, 4.5 mmol) in dry Et_2O at −70 °C was added successively $^iPr_2NH$ (1.4 ml, 10 mmol) and BuLi (2.5 M in hexanes, 4 ml, 10 mmol). After stirring at −70 °C for 1 h, $ClPPh_2$ (1.62 ml, 9 mmol) was added dropwise and the mixture left to warm up to room temperature. The residue after evaporation was Soxhlet extracted with toluene and the concentrated solution filtered through a short silica-gel column. Recrystallization from toluene (30 ml) afforded a first crop (0.7 g) of *trans*-**P$_2$**, m.p. 236–239 °C. Concentration of the solution to 10 ml afforded a second crop of *trans*-**P$_2$** (0.21 g). Slow addition of MeOH (20 ml) to the mother liquor afforded a third crop which proved to be *cis*-**P$_2$** (0.33 g, 13%), m.p. 192–194 °C. Total yield 46%.

trans-**P$_2$**. Anal. Calc. (found) for $C_{32}H_{26}P_2S_4$: C, 64.02 (64.29); H, 4.37 (4.51); P, 10.32 (10.11); S, 21.36 (21.27); ^{1}H NMR ($CDCl_3$, TMS) δ 7.35 (m, 10H, Ph), 2.24 (s, 3H, Me); $^{31}P\{^1H\}$ NMR ($CDCl_3$, H_3PO_4 85%) δ −18.26 ppm (small amounts of the phosphine oxide are observed at 4.27 ppm).

cis-**P$_2$**. Anal. Calc. (found) for $C_{32}H_{26}P_2S_4$: C, 64.02 (64.12); H, 4.37 (4.84); P, 10.32 (8.97); S, 21.36 (20.57); ^{1}H NMR ($CDCl_3$, TMS) δ 7.35 (m, 10H, Ph), 2.24 (s, 3H, Me); $^{31}P\{^1H\}$ NMR ($CDCl_3$, H_3PO_4 85%) δ −18.26 ppm (small amounts of the phosphine oxide are observed at 4.29 ppm).

4.1.2. Tetrakis(diphenylphosphino)tetrathiafulvalene, P$_4$

To a solution of TTF (0.8 g, 4 mmol) in dry THF at −78 °C was added successively $^iPr_2NH$ (2.8 ml, 20 mmol) and BuLi (2.5 M in hexanes, 8 ml, 20 mmol). After stirring for 1 h, $ClPPh_2$ (3 ml, 16 mmol) was added dropwise to the yellow suspension of TTF–Li_4. The solution darkened and an orange precipitate slowly appeared. After stirring overnight, the suspension was evaporated, the residue extracted with CH_2Cl_2, the solution washed with H_2O, dried on $MgSO_4$, concentrated and filtered trough a short silica-gel column. Recrystallization from toluene afforded **P$_4$** as orange crystals (2 g, 53%) m.p. 251–252 °C. ^{1}H NMR ($CDCl_3$, TMS) δ 7.28 (m, Ar). $^{31}P\{^1H\}$ NMR ($CDCl_3$, H_3PO_4) δ −18.2. Anal. Calc. (found) for $C_{54}H_{40}P_4S_4 \cdot C_7H_8$: C, 70.91 (70.73); H, 4.68 (4.64); P, 11.99 (11.95) S, 12.41 (12.45).

4.1.3. Bis[3,4-dimethyl-3'4'-bis(diphenylphosphino)tetrathiafulvalene]rhodium tetrafluoroborate, [o-P$_2$]$_2$Rh$^+$, BF$_4^-$ (1)

A solution containing 0.250 g (0.416 mmol) of *o*-**P$_2$** and 20 ml of CH_3CN was slowly added to a stirred solution of 0.100 g (0.104 mmol) of $[Rh_2(NCCH_3)_{10}][BF_4]_4$ [14] dissolved in 10 ml of CH_3CN. Upon addition, a green solution and a yellow crystalline solid were observed to form. The reaction was stirred for 48 h at room temperature and the yellow solid was collected by filtration, washed with CH_3CN (3 × 5 ml) and vacuum dried; yield 0.220 g (76%). Anal. Calc. (found) for $C_{64}H_{52}BF_4P_4RhS_8$: C, 55.28 (55.34); H, 3.77 (4.06). IR (CsI, Nujol, cm^{-1}): 1505 (w), 1100 (m), 1062 (s), 925 (w), 797 (m), 700 (m), 528 (m), 517 (m), 483 (w), 455 (w), 420 (w). ^{1}H NMR (CD_2Cl_2, δ ppm) 7.46 (t, C_6H_5), 7.20 (t, C_6H_5), 7.11 (d, C_6H_5), 1.82 (s, $-CH_3$). $^{31}P\{^1H\}$ NMR (CD_2Cl_2, H_3PO_4, δ ppm) 50.4 (d, $^1J_{Rh-P}$ = 133.8 Hz). $^{19}F\{^1H\}$ NMR (CD_2Cl_2, δ ppm) −154.9 (s). UV–vis (CH_2Cl_2, λ_{max}) 270, 318, 420. MS *m/z*: 1303 (M^+, 60). CV (0.1 M $TBABF_4/CH_2Cl_2$, vs. Ag/AgCl): $E_{1/2(ox)}$ = +0.63 V, $E_{1/2(ox)}$ = +1.01 V.

4.2. Crystal structure determination of (Z)-P$_2$

Data collection: Enraf–Nonius CAD4F diffractometer; Mo Kα radiation (λ = 0.71073 Å), graphite monochromator, scan type ω–2θ, temperature: 293 K; 2θ range 4–52°, index ranges $0 \le h \le 11$, $-17 \le k \le 16$, $-17 \le l \le 16$, reflections collected 7041, independent reflections 6414 (R_{int} = 0.0146), observed reflections 2880 ($I > 3(\sigma)I$), reflections used in refinements 3038 (parameters 388), absorption correction ψ-scan.

Solution and refinements: direct methods, full matrix, least squares, all atoms except H anisotropic, H atoms introduced at calculated positions, included in structure factor calculation but not refined; weighting scheme $w = 1/(\sigma^2(F) + 0.0025F^2)$. Maximum shift/e.s.d. ratio 0.04; residual electron density 0.54 e Å^{-3}. System used: XTAL3.2 [24]. Anisotropic displacement factors, positional parameters for idealized hydrogen atoms as well as a list of observed and calculated structure factors are available as supplementary data from the authors.

4.3. Crystal structure determination of $[o\text{-}P_2]_2Rh^+$, BF_4^-

Data collection: Rigaku AFC6S diffractometer; Mo Kα radiation ($\lambda_\alpha = 0.71069$ Å), graphite monochromator, scan type ω, temperature: 183 K; 2θ range 4–50°, index ranges $0 < h < 18$, $0 < k < 22$, $-28 < l < 27$, reflections collected 6723, independent reflections 6465 ($R_{int} = 0.163$), observed reflections 2843 ($I > 3(\sigma)I$), reflections used in refinements 2844 (parameters 251), absorption correction ψ-scan.

Solution: direct methods, system: SHELXS [25] and DIRDIF [26].

Refinements: full matrix, least squares. System used: XTAL3.2 [24]. The (o-$\mathbf{P_2}$)Rh$^+$ atoms (except phenyl rings) were refined anisotropically. The BF_4^- anion was found to be severely disordered, with the boron atom and one fluorine atom on the two-fold axis. The other fluorine atoms were then introduced at calculated positions and the whole BF_4^- anion was refined isotropically with the overall thermal parameter and geometrical restraints [27]. Isolated peaks were found in the following Fourier difference. They were attributed to water molecules and could be refined satisfactorily with an isotropic thermal parameter. These disorder problems resulted with an overall poor refinement of the structure. Repeated attempts at higher quality crystals met with failure.

References

[1] M.A. Fox and D.A. Chandler, *Adv. Mater., 3* (1991) 381.
[2] O. Kahn, Y. Pei, M. Verdaguer, J.P. Renard and J. Sletten, *J. Am. Chem. Soc., 110* (1988) 782.
[3] C. Benelli, A. Dei, D. Gatteshi, H.U. Gudel and L. Pardi, *Inorg. Chem., 28* (1989) 3089.
[4] A. Canneschi, D. Gatteschi and P. Rey, *Prog. Inorg. Chem.*, (1991) 331.
[5] K. Inoue and H. Iwamura, *J. Am. Chem. Soc., 116* (1994) 3173.
[6] M. Fourmigué and P. Batail, *Bull. Soc. Chim. Fr., 129* (1992) 29.
[7] M. Fourmigué, S. Jarshow and P. Batail, Proc. XIIth Int. Conf. Phosph. Chem., *Phosphorus Sulfur Silicon, 75* (1993) 175.
[8] D.C. Green, *J. Org. Chem., 44* (1979) 1476.
[9] F. Gerson, A. Lamprecht and M. Fourmigué, *J. Chem. Soc. Perkin Trans. II* (1996) 1409.
[10] S. Jarchow, M. Fourmigué and P. Batail, *Acta Crystallogr. Sect. C:, 49* (1993) 1936.
[11] M. Fourmigué and Y.-S. Huang, *Organometallics, 12* (1993) 797.
[12] M. Fourmigué and P. Batail, *J. Chem. Soc. Chem. Commun.*, (1991) 1370.
[13] (a) E. Aharon-Shalom, J.Y. Becker, J. Bernstein, S. Bittner and S. Shaik, *Tetrahedron Lett.*, (1985) 2783. (b) V.Y. Lee, *Synth. Met., 20* (1987) 161. (c) A.M. Kini, B.D. Gates, M.A. Beno and J.M. Williams, *J. Chem. Soc. Chem. Commun.*, (1989) 169. (d) R.D. McCullough, J.A. Belot and J. Seth, *J. Org. Chem., 58* (1993) 6480.
[14] K.R. Dunbar and L.E. Pence. *Inorg. Synth., 29* (1992) 182.
[15] J.H. Matonic, S.-J. Chen, L.E. Pence and K.R. Dunbar, *Polyhedron, 11* (1992) 541.
[16] B.J. Hathaway, D.G. Holah and A.E. Underhill. *J. Chem. Soc.*, (1962) 2444.
[17] A. deRenzi, A. Panunzi and A. Vitagliano. *J. Chem. Soc. Chem. Commun.*, (1976) 47.
[18] R.R. Thomas and A. Sen. *Inorg. Synth., 26* (1989) 128.
[19] B. Garreau, D. de Montauzon, P. Cassoux, J.-P. Legros, J.-M. Fabre, K. Saoud and S. Chakroune, *New J. Chem., 19* (1995) 161.
[20] J. Ippen, C. Tao-pen, B. Starker, D. Schweitzer and H.A. Staab, *Angew. Chem. Int. Ed. Engl., 19* (1980) 67.
[21] (a) K. Boubekeur, P. Batail, F. Bertho and A. Robert, *Acta Crystallogr. Sect. C:, 47* (1991) 1109. (b) K. Boubekeur, C. Lenoir, P. Batail, R. Carlier, A. Tallec, M.-P. Le Paillard, D. Lorcy and A. Robert, *Angew. Chem. Int. Ed. Engl., 33* (1994) 1379.
[22] K. Lerstrup, I. Johannsen and M. Jørgensen, *Synth. Met. B, 27* (1988) 9.
[23] A. Mas, J.-M. Fabre, E Torreilles, L. Giral and G. Brun, *Tetrahedron Lett.*, (1977) 2579.
[24] S.R. Hall, H.D. Flack and J.M. Stewart (eds.), XTAL3.2 *Reference Manual*, Universities of Western Australia, Geneva and Maryland, 1992.
[25] G.M. Sheldrick, in G.M. Sheldrick, C. Kruger and R. Goddard (eds.), *Crystallographic Computing 3*, Clarendon Press, Oxford, 1985, pp. 175–189.
[26] R.T. Beurskens, DIRDIF: *Direct Methods for Difference Structure, An Automatic Procedure for Phase Extension; Refinement of Difference Structure Factors*, Technical Support, 1984.
[27] J. Waser, *Acta Crystallogr., 15* (1963) 558.